Nanoscale plasmon waveguide including cavity resonator

2009 J. Phys.: Condens. Matter 21 375301

(http://iopscience.iop.org/0953-8984/21/37/375301)

J. Phys.: Condens. Matter **21** (2009) 375301 (6pp) doi:10.1088/0953-8984/21/37/375301

Nanoscale plasmon waveguide including cavity resonator

A Noual, Y Pennec, A Akjouj[1], B Djafari-Rouhani and L Dobrzynski

Institut d'Electronique, de Microélectronique et de Nanotechnologie (IEMN), UMR CNRS 8520, UFR de Physique, Université des Sciences et Technologies de Lille, F-59655 Villeneuve d'Ascq Cédex, France

E-mail: Abdellatif.Akjouj@univ-lille1.fr

Received 15 April 2009, in final form 13 July 2009
Published 17 August 2009
Online at stacks.iop.org/JPhysCM/21/375301

Abstract

The propagation and filtering of surface plasmon polaritons in metal–insulator–metal nanosandwiches are investigated by using finite-difference time domain simulation. We study the optical transmission of a nanoscale waveguide coupled to a cavity situated either in the vicinity or in the interior of the waveguide. Depending on whether the cavity is inside or at the side of the waveguide, the transmission spectrum displays respectively peaks or dips which occur at the same frequencies. We study the dip and peak frequencies in the transmission spectrum as a function of the geometrical parameters of the cavity and the thickness of the metallic gap separating the guide from the cavity.

(Some figures in this article are in colour only in the electronic version)

The realization of a strongly confined light beam with sufficiently low propagation loss for practical applications is of central importance in integrated nanophotonics. A light wave coupled to free-electron oscillations at metal–dielectric interfaces, known as surface plasmon polaritons (SPPs), can be laterally confined in a nanoscale domain [1]. This attracts tremendous research interest in constructing novel waveguide structures with nanometric cross sections. Several plasmonic waveguiding structures have been proposed such as metallic nanowires [2], metallic nanoparticle arrays [3–5] and V grooves in metal substrates [2, 6]. Some of these structures focus the light into the dielectric core in a metal–insulator–metal (MIM) sandwich and allow the manipulation and transmission of light at the nanoscale. MIM-based plasmon slot waveguides have been shown to provide both long-range propagation and subwavelength spatial confinement [7]. Miyazaki and Kurokawa have proposed a nanosheet plasmon cavity, which utilizes a dielectric thin film as a gap, and demonstrated controlled plasmon resonances in 3 nm wide gaps with systematic experiments [8]. MIM waveguides are promising structures for the design of nanoscale all-optical devices as the numerical and experimental investigations show strong localization and zero bend losses as well as relatively simple fabrication [8–11]. The structure presented here is closely linked to new progress in the nanotechnology experimental field. Therefore, processes of fabrication in the nanometer scale should be theoretically improved, such as, for example, how fabrication inaccuracies influence the optical properties [8, 11].

In this paper, we investigate nanocavity resonator filters in a two-dimensional plasmon–polariton MIM waveguide, using a finite-difference time domain (FDTD) method [12]. The effect of coupling the nanowaveguide to a cavity is to induce peaks or dips (or zeros) in the transmission coefficient depending on whether the cavity is situated inside or in the vicinity of the waveguide. The main purpose of this paper is to discuss the possibility of a selective or rejective peak in the transmission by choosing appropriately the geometrical parameters of the structure. This enables us to get, in particular, a selective peak in the transmission spectrum for a simple cavity device.

The dielectric function of the metal (silver) is described by the lossy Drude model:

$$\varepsilon(\omega) = \varepsilon_\infty - \frac{\omega_p^2}{\omega^2 + i\Gamma\omega} \tag{1}$$

where ε_∞ is the relative permittivity at infinite frequency, ω_p is the plasma frequency and Γ is the collision frequency. We choose $\varepsilon_\infty = 12.5$, $\omega_p = 2.05 \times 10^{16}$ rad s^{-1} and

[1] Author to whom any correspondence should be addressed.

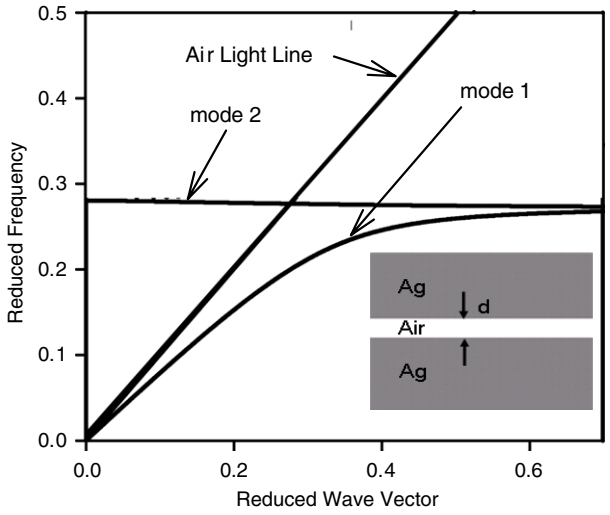

Figure 1. Dispersion relations (reduced frequency versus reduced wavevector) for Ag/air/Ag waveguide. The structure is shown in the inset. The width of the waveguide is denoted by $d = 50$ nm.

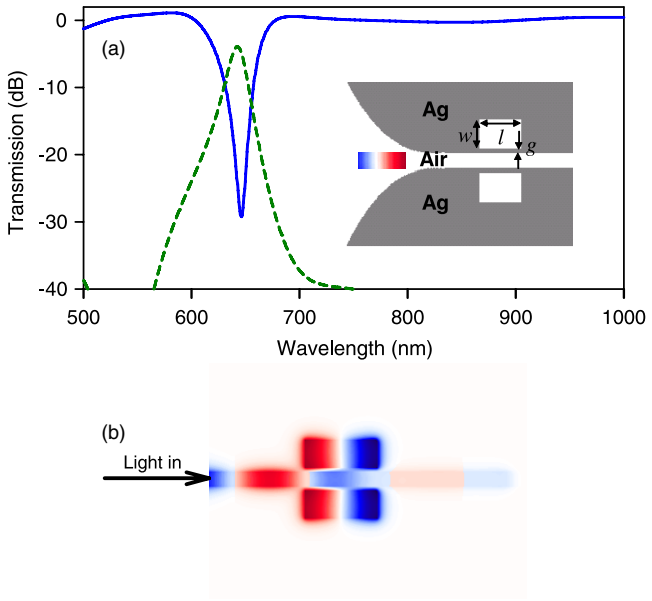

Figure 2. (a) Transmission (solid line) and reflection spectra (dashed line) as a function of the wavelength for the system inserted in this figure with the parameters $l = 240$ nm, $w = 100$ nm and $g = 17$ nm. The transmission and reflection are normalized with respect to the output and input powers of the straight waveguide without rectangular cavities. A schematic of an Ag/air/Ag-based rectangular nanocavity is shown in the inset. (b) Map of magnetic field for monochromatic incident radiation at the wavelength of the zero of transmission ($\lambda = 646$ nm).

$\Gamma = 1.0 \times 10^{14}$ rad s^{-1} for the Drude model, which fit the experimental data [13] quite well. The waveguide width of 50 nm is one order of magnitude smaller than the wavelength in air (see figure 1).

According to the symmetry of the perfect waveguide, the propagating waves can be distinguished between symmetric and antisymmetric modes. The well-known solutions of such waves in the perfect waveguide are [14]

$$\tan(\alpha_2 d) = -\frac{\varepsilon_1}{\varepsilon_2}\frac{\alpha_2}{\alpha_1} \tag{2}$$

for the symmetric mode and

$$\coth(\alpha_2 d) = -\frac{\varepsilon_1}{\varepsilon_2}\frac{\alpha_2}{\alpha_1} \tag{3}$$

for the antisymmetric mode, with

$$\alpha_1 = \left(k_\parallel^2 - \frac{\omega^2 \varepsilon_1}{c^2}\right), \tag{4}$$

$$\alpha_2 = \left(k_\parallel^2 - \frac{\omega^2 \varepsilon_2}{c^2}\right). \tag{5}$$

Here $k_\parallel$ is the wavevector parallel to the guide, $\varepsilon_2 = 1$, $\varepsilon_1 = \varepsilon(\omega)$, d is the width of the waveguide and c is the light velocity.

Figure 1 presents the dispersion of surface plasmon modes (the dimensionless frequency (ω/ω_p) versus the reduced wavevector $(k_\parallel d)$) in a vacuum slab sandwiched between two semi-infinite media made of Ag.

The two dispersion curves 1 and 2 correspond to modes confined in the dielectric region and decaying exponentially on both sides into the interior of the metals. Both branches have TM polarization, which means that the magnetic field is perpendicular to the wave propagation direction and are respectively antisymmetric (branch 1) and symmetric (branch 2) with respect to the plane symmetry of the structure.

In our study, the antisymmetric mode, for which the waveguide is monomode in a large reduced frequency range (0.09–0.23), is excited. Let us notice that this frequency range corresponds to the wavelength range of (400–1000 nm).

The inset of figure 2(a) shows the geometry of the structure which consists of rectangular resonator cavities coupled to a bus waveguide. The coupling between the cavity resonators and the input waveguide depends on the separation between them by a metallic gap of thickness g. l and w are the length and the width of the cavities. The embedded medium is the metal (silver). The waveguide and the cavities are made of the same insulator (air in our case). We refer to the cavity resonator dimensions by (w, l) with both values presented in nanometers.

Calculations are performed using the finite-difference time domain (FDTD) method which solves Maxwell's equations [12, 15] by discretizing both time and space and by replacing derivatives with finite differences. Our calculation is performed in a two-dimensional (2D) box (along x and y axes) with perfect matching layer (PML) conditions applied at the boundaries of the box, in order to avoid reflections of outgoing waves [16]. The structure is supposed to be infinite along the z direction. Space is discretized in both x and y directions using a mesh interval equal to $x = y = 3$ nm. The equation of motion is solved with a time integration step $\Delta t = 3 \cdot 10^{-3}$ fs and a number of time steps equal to 2^{20} which is the necessary tested time for a good convergence of the numerical calculation.

We choose to study the transverse magnetic (TM) polarization with the electric field **E** belonging to the

(x, y) plane of the figure and the magnetic field **H** being perpendicular to this plane. The incoming pulse is generated at the left end of the waveguide, inside the taper region, by a current source parallel to the x axis and having a Gaussian profile along the x direction. The current is generated during a short period of time in such a way as to excite the electromagnetic waves in the frequency domain of interest. The coupling loss between the light source and the waveguide is equal to -5 dB. The transmitted signal, probed at the right end of the waveguide, is recorded as a function of time, integrated over the cross section of the waveguide and finally Fourier-transformed to obtain the transmission coefficient versus the wavelength. All the transmission spectra are normalized with respect to the one corresponding to a perfect (without nanocavity resonator) waveguide. The transmission is reported in decibels (dB) as a function of the wavelength (in nanometers) of light in air.

In figure 2(a) we present the calculated transmission (solid line) and reflection (dashed line) spectra as a function of the wavelength for two nanocavities symmetrically attached to the waveguide with $l = 240$ nm, $w = 100$ nm and $g = 17$ nm. It is well known that such a cavity possesses several surface plasmon modes, whose number and positions depend on the cavity aspect ratio, volume and surrounding medium permittivity [17]. For the present geometry, only one resonance appears in the range of the wavelength computed, as shown in figure 2(a). The interaction between the waveguide and the nanocavity through the metallic gap creates a -30 dB dip in the transmission at the wavelength of 646 nm in the transmission spectrum (see figure 2(a)), thus creating a rejective filter. The reflection coefficient, evaluated at the entrance of the waveguide, amounts to 60% which means that approximately 40% of the input signal has been absorbed inside the two cavities. Let us stress that these estimations are not significantly altered by the absorption during the propagation along the waveguide because the latter attenuation can be evaluated only to -1.15 dB μm^{-1}. One can notice that such filtering phenomena have already been observed using micro-ring or micro-disc resonator devices [18, 19]. In [18] and [19], the surface cavity varies from 0.5 to 3 μm^2 and the quality factor is about 30. The current challenge is to produce resonators which offer very good properties such as narrow bandwidth filtering and high quality factors. Small devices permit the integration of these resonators with other nanometer-sized components to fabricate photonic integrated circuits. In our work, the surface cavity is about 0.024 μm^2 and the quality factor can reach a value of 50 (see figure 4).

The dip in the transmission spectrum occurs at the wavelength of the plasmon–polariton eigenmode (resonance) of the cavity. The latter is calculated in the following way: a temporal pulse is created in an isolated cavity inside a thick metal, then the electromagnetic field is probed at different positions in the cavity during the time, and finally a Fourier transform of the temporal response is made to obtain the frequency spectrum. Actually, the wavelength of the dip in the transmission is slightly shifted with respect to the resonance wavelength of the cavity. In the same way, we have also noticed small changes of the wavelength (frequency)

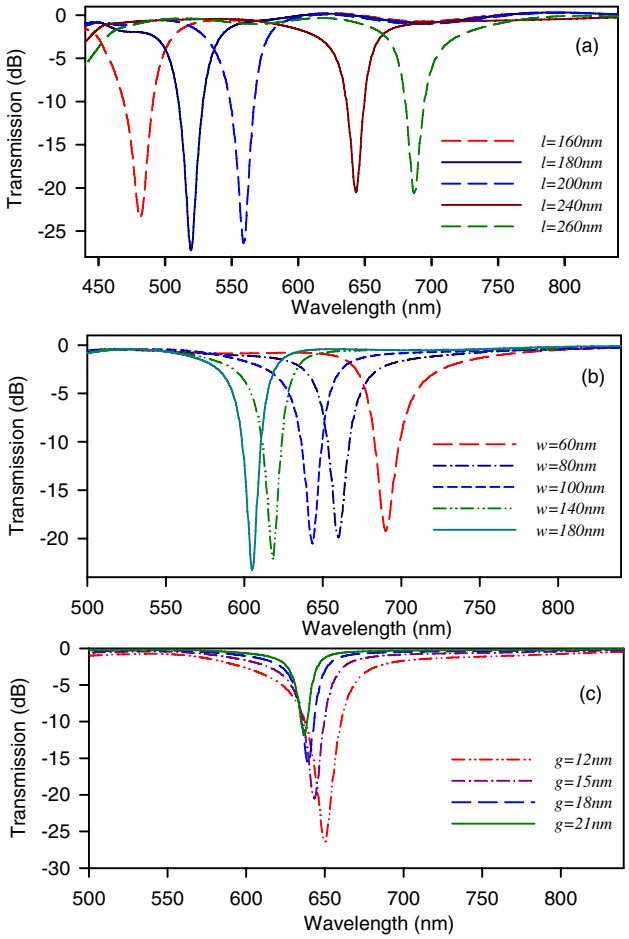

Figure 3. (a) Evolution of the peak of the transmission spectra as a function of the wavelength for different values of the cavity length l with $w = 100$ nm and $g = 17$ nm. (b) The same as in (a) but for different values of the cavity width w with $l = 240$ nm and $g = 17$ nm. (c) The same as in (a) but for different values of the metallic gap g of the cavity with $l = 240$ nm and $w = 100$ nm.

of the transmission dip when the cavity is rotated by $\pi/2$. Nevertheless, such variations remain small in comparison with the full width at half-maximum (FWHM) of the resonance. For $l = 240$ nm and $w = 100$ nm, the resonant frequency is equal to 646 nm and the FWHM $\Delta\lambda = 17$ nm, whereas for $l = 100$ nm and $w = 240$ nm, the resonant frequency is equal to 644 nm and the FWHM $\Delta\lambda = 13$ nm. Finally, let us notice that the different coupling conditions caused by the rotating of the cavity also affect the quality factor and the depth of the dip.

The map corresponding to the magnetic field for the resonance mode ($\lambda = 646$ nm) is shown in figure 2(b). One observes a strong interaction between the waveguide and the cavity which leads to the excitation of a plasmon mode essentially confined at the boundaries of the nanocavity, which in turn produces the reflection and the absorption of the incident field. The plasmon mode is well confined inside the nanocavities and is not transmitted. Let us notice that the eigenvector is symmetrical with respect to the axis parallel to the small side of the cavity and antisymmetrical with respect to the axis parallel to the large side of the cavity.

In figure 3, we study the evolution of the above wavelengths (cavity eigenmode as well as the wavelength of

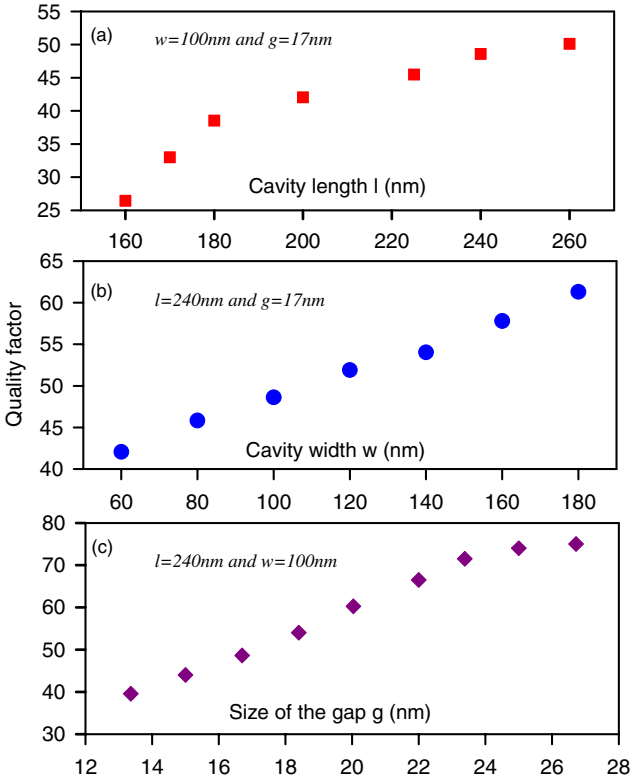

Figure 4. Quality factor versus l assuming $g = 17$ nm and $w = 100$ nm (a) versus w assuming $g = 17$ nm and $l = 240$ nm (b) and versus g assuming $l = 240$ nm and $w = 100$ nm (c).

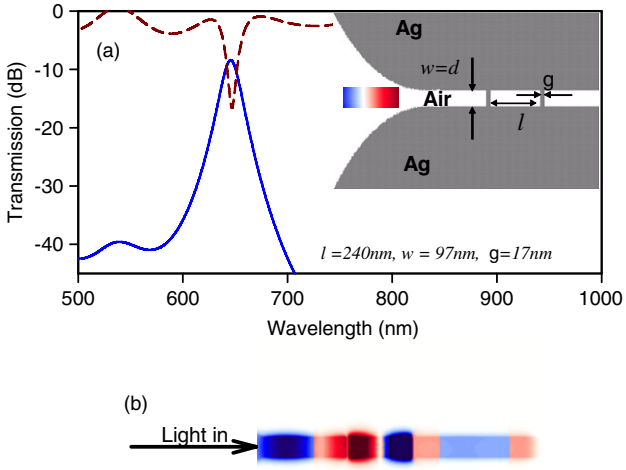

Figure 5. (a) Transmission spectrum versus the wavelength using the parameters $l = 240$ nm, $w = 97$ nm and $g = 17$ nm. A schematic view of an Ag/air/Ag structure with a rectangular cavity inside the nanowaveguide is shown in the inset. (b) Map of magnetic field for monochromatic incident radiation at the wavelength of the maximum of transmission ($\lambda = 645$ nm).

the dip in the transmission coefficient) with the geometrical parameters l and w of the cavity. Let us recall that the interaction between the antisymmetric mode of the waveguide and the plasmon mode of the cavity through the metallic gap displays a transmission dip with attenuation exceeding 20 dB. In figure 3(a) the transmission coefficient is given for different lengths l ($l = 160, 180, 200, 240$ and 260 nm) of the cavity when the width w is taken equal to 100 nm. One can observe that increasing the length l of the nanocavity shifts the mode to the higher wavelengths. Figure 3(b) shows the transmission spectrum for different values of $w = 60, 80, 100, 140$ and 180 nm, the length l being taken equal to 240 nm. Unlike the previous case, here the increase in the width w pushes the mode to lower wavelengths although the variation in the resonance wavelength is weaker than in figure 2(a). These apparently opposite behaviors will be discussed below in the frame of another example (figure 7). Figure 3(c) shows the transmission spectrum for different values of $g = 12, 15, 18$ and 21 nm, the length l and the width w being taken equal to 240 nm and 100 nm, respectively.

In figure 4, we study the influence of the geometrical parameters l, w and g on the quality factor Q of the resonance (dip). The quality factor is defined by the equation: $Q = \frac{\lambda_r}{\Delta\lambda}$, where λ_r is the resonant wavelength and $\Delta\lambda$ is the full width at half-maximum. Figures 4(a) and 4(b) show that the increase of the length l or the width w leads to a higher quality factor Q. The same trend is observed when the metallic gap between the waveguide and the nanocavity is increased (figure 4(c)). This latter result is strongly correlated to a weaker coupling between the cavities and the waveguide. However, since the penetration of the surface plasmon into the metal is about 20 nm, the thickness g should not exceed this range; otherwise the coupling between the cavities and the guide will not be sufficiently strong. Finally, let us notice that, for the nanocavity of length $l = 240$ nm and width $w = 100$ nm, the resonance is at a wavelength of 646 nm, a quality factor of 50 and a modal surface of 0.024 μm^2. Although these considerations may improve the Q factor, they rely of course on good nanoprecisions of the device.

With this kind of resonant lateral cavities, one may have zeros of transmission corresponding to a cavity wavefunction vanishing inside the main guide. Now, we consider another type of cavity inserted inside the main waveguide (see the inset in figure 5). This cavity is made out of one piece of air separated from the rest of the main guide by two thin pieces of metal. These pieces of metal reject all wave frequencies, but transmit those corresponding to the cavity eigenmodes. The corresponding transmission spectrum is presented in figure 5(a) with the following parameters: $w = 97$ nm, $l = 240$ nm and $g = 17$ nm. One can notice that in this case all wavelengths are reflected except the one associated with the excitation of the cavity. This behavior is similar to those of an electron quantum double barrier [20]. The wavelength of the resonance mode, which is equal to 645 nm, remains identical to that obtained for a dip when the cavity was located outside the waveguide. This type of structure allows us to create a selective filter. In figure 5(a), the transmission peak still remains relatively small (about 40%) whereas the reflection coefficient falls down to approximately 15%. This means that a large amount of the incident energy is absorbed inside the cavities during the process of transmission.

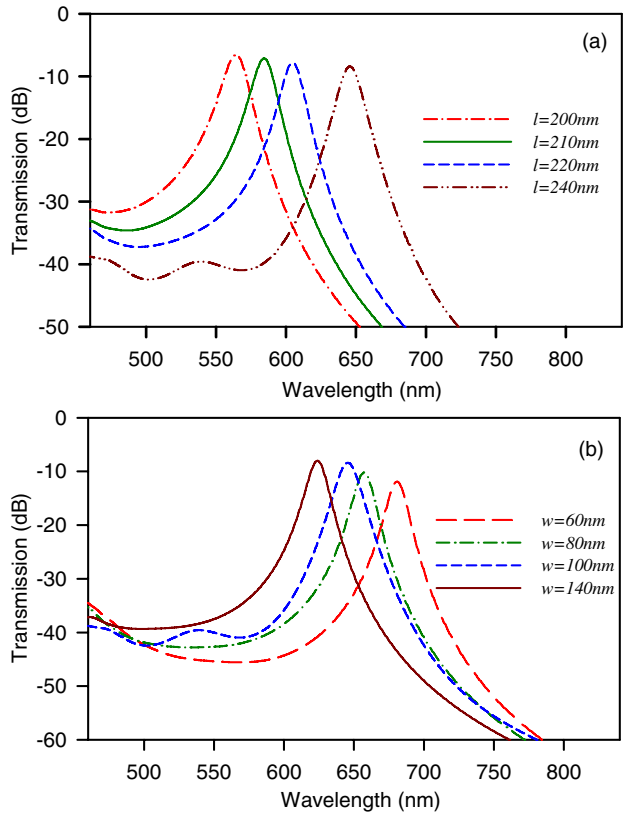

Figure 6. (a) Evolution of the peak of the transmission spectra as a function of the wavelength for different values of the cavity length l with $w = 97$ nm and $g = 17$ nm. (b) The same as in (a) but for a cavity width w with $l = 240$ nm and $g = 17$ nm.

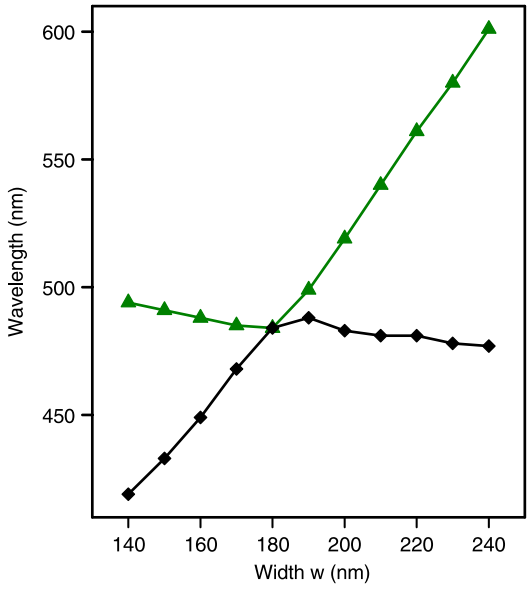

Figure 7. Evolution of the wavelength of dips in the transmission spectra versus w for $l = 180$ nm and $g = 17$ nm. The evolution is presented in a case where the cavities display two eigenmodes in the range of studied wavelength. Diamonds (in black) correspond to mode 1 and triangles (in green) correspond to mode 2.

The map corresponding to the magnetic field for the transmitted mode ($\lambda = 645$ nm) is shown in figure 5(b) and shows a strong interaction between the waveguide and the

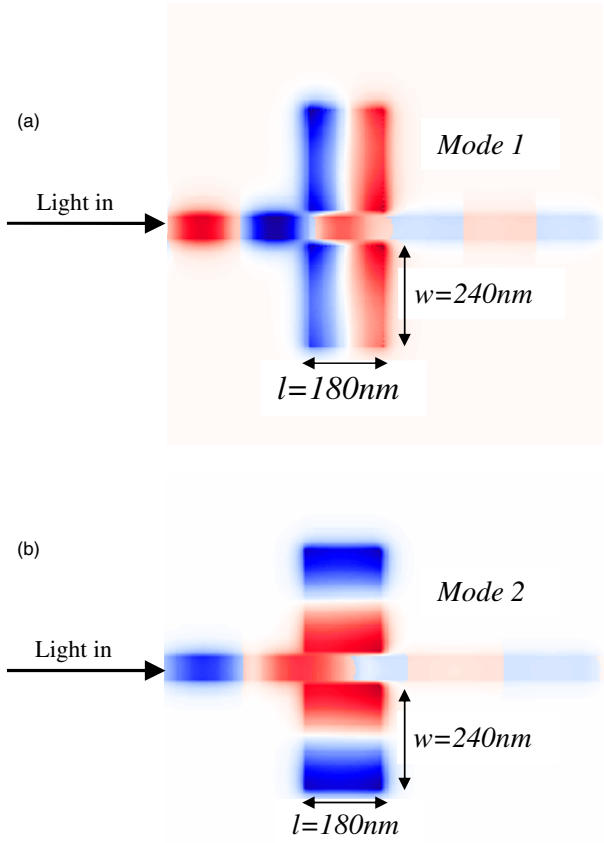

Figure 8. Maps of magnetic fields for monochromatic incident radiation at the wavelengths of the zeros of transmission coefficient ($\lambda = 601$ nm (a) and $\lambda = 477$ nm (b)). The geometrical parameters of the cavity are $l = 180$ nm and $w = 240$ nm.

nanocavity. The symmetry of the eigenmode is the same as in figure 2(b).

The evolution of the selected frequency as a function of the geometrical parameters is studied in figure 6. In figure 6(a) the transmission coefficient is given for different lengths l ($l = 200, 210, 220$ and 240 nm) of the cavity when the width w is taken equal to 97 nm. One can observe that increasing the length l of the nanocavity shifts the mode to the higher wavelengths. Figure 6(b) shows the transmission spectrum for different values of $w = 80, 90, 110$ and 123 nm, the length l being taken equal to 240 nm. Unlike the previous case, here the increase in the width w pushes the mode to lower wavelengths although the variation in the resonance wavelength is weaker than in figure 6(a). These trends are in agreement with those presented in figure 3.

Finally, we study the evolution of the resonance frequencies in a case where the cavities displays two eigenmodes in the range of studied wavelengths. We start from a square cavity, with $l = w = 180$ nm, and then modify the length w around this value, from 140 to 240 nm. The resonance frequencies, deduced from the dips in the transmission coefficient (figure 2(a)), are shown in figure 7 as a function of w. We call respectively 1 and 2 the lower and higher modes in figure 7. These two modes can be distinguished one from each other by their characteristics, namely the localization of mode 1 (resp. 2) occurs mainly

along the large (small) sides of the cavity; also mode 1 (resp. 2) is antisymmetrical (resp. symmetrical) with respect to the cavity axis parallel to the small side, whereas it is symmetrical (resp. antisymmetrical) with respect to the cavity axis parallel to the large side. An example of the maps of the magnetic field for both modes 1 and 2 is presented in figure 8 with $l = 180$ nm and $w = 240$ nm. From this point of view, the mode discussed in figures 2–5 has the characteristic of mode 2. In figure 7, one can notice that the wavelength of mode 1 increases when w increases from 140 to 180 nm and then displays an almost constant or a small decreasing behavior when w exceeds 180 nm. A complementary behavior is obtained for mode 2 whose wavelength changes slightly for w below 180 nm whereas it increases when w exceeds 180 nm. Finally, let us notice that similar trends are observed either by rotating the side cavities by $\pi/2$ or by putting the cavity inside the waveguide and looking at the transmission peak, or by calculating directly the resonances of an isolated cavity. However, the quantitative results may differ by a small amount in each case due to the different types of interaction between the guide and the cavities. When the cavity is rotated by $\pi/2$, the frequency shift of the resonance remains smaller than the deep width.

In summary, we have reported a numerical investigation of the transmission through a plasmonic waveguide coupled to lateral or inserted cavities. We show the possibility of rejective or selective filters for plasmon waves. This enables us to get, in particular, a peak or dip in the transmission spectrum. Moreover, an appropriate choice of the geometrical parameters enables us to choose the filtering frequency at will for specific applications.

References

[1] Barnes W L, Dereux A and Ebbesen T W 2003 *Nature* **424** 824–30
[2] Berini P 2000 *Phys. Rev.* B **61** 10484–503
[3] Quintin M, Leinter A, Krenn J R and Aussenegg F R 1998 *Opt. Lett.* **23** 1331–3
[4] Maier S A *et al* 2003 *Nat. Mater.* **2** 229–32
[5] Dobrzynski L, Akjouj A, Djafari-Rouhani B, Vasseur J O, Bouazaoui M, Vilcot J P, AlWahsh H, Zielinski P and Vigneron J P 2004 *Phys. Rev.* E **69** 035601
[6] Pile D E P and Gramotnev D K 2005 *Appl. Phys. Lett.* **30** 1186–8
[7] Dionne J A, Sweatlock L A, Atwater H A and Polman A 2005 *Phys. Rev.* B **72** 075405
[8] Miyazaki H T and Kurokawa Y 2006 *Phys. Rev. Lett.* **96** 097401
[9] Dionne J A, Sweatlock L A, Atwater H A and Polman A 2006 *Phys. Rev.* B **73** 035407
[10] Kurokawa Y and Miyazaki H T 2007 *Phys. Rev.* B **75** 035411
[11] Yu Z, Veronis G, Fan S and Brongersma M L 2008 *Appl. Phys. Lett.* **92** 041117–9
[12] Taflove A 2000 *Computational Electrodynamics: the Finite Difference Time Domain Method* 2nd edn (Norwood: Artech House)
[13] Palik E D 1985 *Handbook of Optical Constants of Solids* (New York: Academic)
[14] Bah M L, Akjouj A and Dobrzynski L 1992 *Surf. Sci. Rep.* **16** 95–131
[15] Yee K S 1966 *IEEE Trans. Antennas Propag.* **14** 302–7
[16] Berenger J P 1994 *J. Comput. Phys.* **114** 185
[17] Kottmann J P, Martin O J F, Smith D R and Schultz S 2001 *Phys. Rev.* B **64** 235403
[18] Xiao S, Liu L and Qiu M 2006 *Opt. Express.* **14** 2932
[19] Hosseini A and Massoud Y 2007 *Appl. Phys. Lett.* **90** 181102
[20] Esaki L 1989 *Proc. 3rd Int. Symp. Foundations of Quantum Mechanics (Tokyo)* pp 369–82